NANO LETTERS

pubs.acs.org/NanoLett

Letter

Directionally-Resolved Phononic Properties of Monolayer 2D Molybdenum Ditelluride ($MoTe_2$) under Uniaxial Elastic Strain

Zhewen Yin, Wyatt Panaccione, Anjun Hu, Ossie R. T. Douglas, Md Rubayat-E Tanjil, Yunjo Jeong, Huijuan Zhao, and Michael Cai Wang*

Cite This: *Nano Lett.* 2023, 23, 11763−11770

Read Online

ACCESS | Metrics & More | Article Recommendations | Supporting Information

ABSTRACT: Understanding the phonon characteristics of two-dimensional (2D) molybdenum ditelluride ($MoTe_2$) under strain is critical to manipulating its multiphysical properties. Although there have been numerous computational efforts to elucidate the strain-coupled phonon properties of monolayer $MoTe_2$, empirical validation is still lacking. In this work, monolayer 1H-$MoTe_2$ under uniaxial strain is studied via *in situ* micro-Raman spectroscopy. Directionally dependent monotonic softening of the doubly degenerate in-plane E^1_{2g} phonon mode is observed with increasing uniaxial strain, where the E^1_{2g} peak red-shifts -1.66 ± 0.04 cm^{-1}/% along the armchair direction and -0.80 ± 0.07 cm^{-1}/% along the zigzag direction. The corresponding Grüneisen parameters are calculated to be 1.09 and 0.52 along the armchair and zigzag directions, respectively. This work provides the first empirical quantification and validation of the orientation-dependent strain-coupled phonon response in monolayer 1H-$MoTe_2$ and serves as a benchmark for other prototypical 2D transition-metal tellurides.

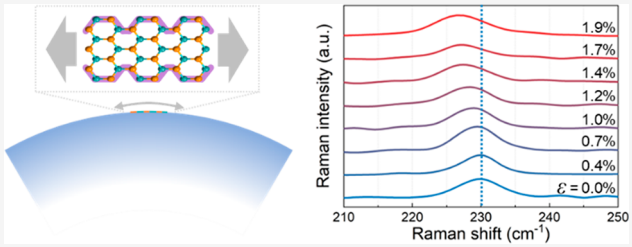

KEYWORDS: *molybdenum ditelluride, strain engineering, phonon evolution, Grüneisen parameter, Raman spectroscopy*

Transition-metal tellurides, as the relatively heavier members of the atomically thin two-dimensional (2D) transition-metal dichalcogenide (TMDC) family, are the only TMDCs with a stable metalloid chalcogen (tellurium). In particular, molybdenum ditelluride ($MoTe_2$) is of great interest for its ambient-stable yet readily and reversibly tunable polymorphs, each with drastically different multiphysical and highly layer-dependent intrinsic properties. Evidence of exotic phenomena such as Rydberg excitons,[1] edge supercurrents,[2,3] switchable ferromagnetic domains,[4] and fractional quantum anomalous Hall states[5] have also been discovered in various phases of $MoTe_2$. The most stable polymorph of $MoTe_2$ is the semiconducting 2H phase, with an indirect band gap of ∼0.9 eV in its few-layered (2H-) form and a direct band gap of ∼1.1 eV in its monolayer (1H-) form.[6−8] This 2H-phase exhibits a trigonal-prismatic crystal structure with the space group $P6_3/mmc$ and point group D_{3h}.[9,10] Additionally, the other polymorphs of $MoTe_2$ include 1T, 1T′, T_d, and 3R phases.[11,12] These diverse $MoTe_2$ polymorphs, each with unique crystal structures, symmetries, and intrinsic properties, allow a myriad of potential applications spanning optoelectronics, superconductors, chemical sensors, neuromorphic elements, and quantum devices.[3,13−17]

The phononic properties of $MoTe_2$ reflect the structural variations among different polymorphic phases. Phonon evolution modulated by strain is preferred owing to its nondestructive attributes and its pronounced reversibility under the constraints of ambient conditions.[18] In comparison, other strategies to induce phase transition in $MoTe_2$ have included the tuning of Te vacancies, such as through controlled chemical vapor deposition (CVD),[19] alloying,[20] laser irradiation,[21,22] electrostatic doping,[23,24] plasma etching,[25] thermal treatment,[6,26] etc. These methods are effective in tuning the phonon status but permanently affect materials' lattice structures and stoichiometric compositions. Thus, gaining insight into the strain−phonon coupling properties of $MoTe_2$ can lead to a facile way for low-power control over various states of phonons.

To date, only very few experimental studies have reported on the strain-induced phonon evolution in $MoTe_2$, with all of these findings being limited to multilayer $MoTe_2$. These studies yielded disparate findings, including both the presence and absence of phase change from 2H to 1T′ under uniaxial or biaxial tensile strains (0.2−4.5%).[18,27−29] Another type of phase change from 1T′ to a quoted semiconducting phase was also reported under 0.33% uniaxial tensile strain.[30] Computationally, density functional theory (DFT) calculations have been adopted to study the energy barrier variations between 2H and 1T′ phases under various strain conditions.[31,32] The

Received: September 26, 2023
Revised: November 28, 2023
Accepted: November 28, 2023
Published: December 15, 2023

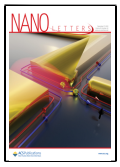

2H to 1T′ phase transition has been consistently found to be more accessible under uniaxial tension along the armchair direction compared to the zigzag direction. The evolution in phonon dispersion of the 2H/1H phase[33−36] and 1T′ phase[37] has also been reported, but only under biaxial tension. There are quantitative discrepancies between different DFT studies due to the varying selection of the DFT solver and calculation setup. Thus far, the evolution in the phonon dispersion of 1H/2H-$MoTe_2$ under uniaxial tension has not been reported.

Furthermore, the mismatch in the number of $MoTe_2$ layers studied in experimental versus computational studies and their respective findings further exacerbate the discrepancies in the literature. While most of the computational studies have been based on monolayer $MoTe_2$, all of the experimental measurements to date have only been done on flakes ranging between 2 and 100 layers.[18,27−30] For these thicker crystals, interlayer slippage may occur and affect the coherency of strain transfer from the substrate.[28] Therefore, strictly isolating $MoTe_2$ crystals that are monolayers is critical for obtaining reliable strain−phonon coupling results. Moreover, the hexagonal primitive unit cell and trigonal-prismatic coordination of 2H-$MoTe_2$ means that the in-plane mechanical loading response of 2H-$MoTe_2$ is directionally dependent. However, none of the reported experimental results thus far distinguished the lattice orientation. To resolve these knowledge gaps, it is imperative to empirically validate the directionally dependent strain−phonon coupling within monolayer 1H-$MoTe_2$.

In this work, *in situ* micro-Raman spectroscopy was used to monitor the phonon evolution of monolayer 1H-$MoTe_2$ as a function of the uniaxial tensile strain. For the first time, a consistent directionally dependent, monotonic red-shift of the in-plane vibrational E^1_{2g} phonon mode was empirically substantiated for both armchair and zigzag directions. Such strain−phonon coupling reveals the potential applications of these 2D materials in detecting minuscule structural deformations *in situ*, conducive to the development of nanoscale sensors for mechanical, optical, electrical, and biological applications.[30,38−40] By quantifying the E^1_{2g} mode Grüneisen parameter based on the strain-coupled phonon response, this work sets a benchmark for the strain-engineering of $MoTe_2$ and is generalizable to other 2D tellurides. Understanding the phononic behaviors of these 2D materials is essential for harnessing their unique properties for novel optoacoustic and thermomechanical applications.

Among all the currently isolatable 2D TMDCs, $MoTe_2$ exhibits the lowest energy difference (43 meV) between the two most stable semiconducting α-form (1H or 2H) and semimetallic β-form (1T′) phases,[31] with its phononic properties being highly sensitive to external fields. Under ambient conditions, hexagonal 2H-$MoTe_2$ (denoted as 1H-$MoTe_2$ in the monolayer form) is the most stable configuration[41] of $MoTe_2$ where the Te atoms are in trigonal-prismatic coordination around the Mo atoms with a primitive hexagonal unit cell (Figure 1a).

As 2D monolayer crystals are considered "all surface" materials, controlled uniaxial strain could be introduced to monolayer $MoTe_2$ by straining a deformable substrate underneath, where the properties of the substrate play an important role in effective strain transfer and the corresponding phononic coupling with the $MoTe_2$. According to shear-lag analysis, it has been theoretically established[42] and experimentally verified[43] that interfacial strain transfer efficiency has a positive correlation with the shear modulus of the substrate,

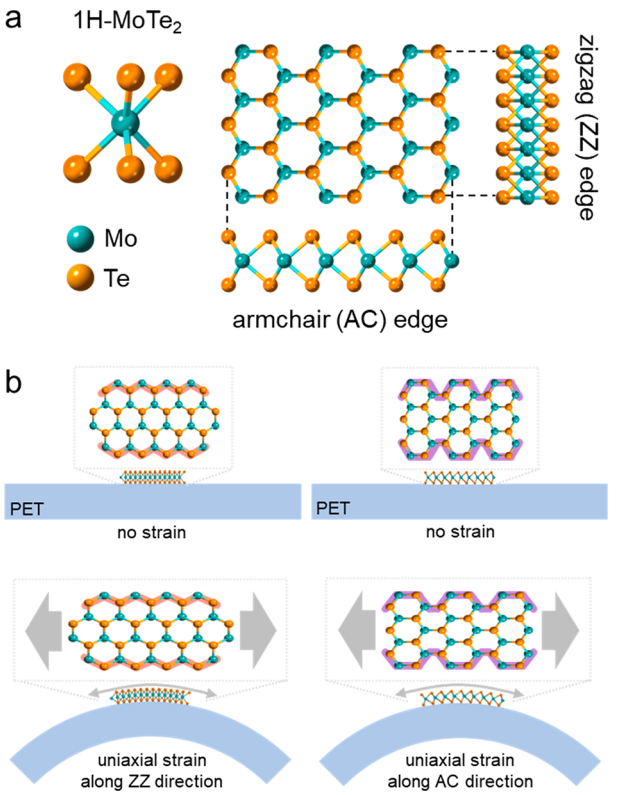

Figure 1. (a) Crystal structure of the 1H phase monolayer $MoTe_2$. The 1H phase is semiconducting with trigonal-prismatic coordination. (b) Schematic of monolayer 1H-$MoTe_2$ (∼0.67 nm thick, 20−50 μm in lateral size) aligned on PET substrates (∼0.79 mm thick, 50 mm long) under unstrained (upper) and uniaxially strained (lower) configurations along the zigzag (left) and armchair (right) crystal directions. Due to the minuscule ratios between the monolayer 1H-$MoTe_2$ and PET sheet in both lateral size (∼4×10^{-4}) as well as thickness (∼9×10^{-7}), the 1H-$MoTe_2$ adhered to the PET surface is considered under uniaxial applied tensile strain when PET sheets are bent.

which is determined by the Young's modulus and Poisson ratio. The Poisson ratio also factors into the calculation of the Grüneisen parameter. Substrates with high Young's moduli and strong adhesion allow the strain to be effectively transferred to the surface 2D materials, thus enabling a higher range of strain modulation. 1H-$MoTe_2$ monolayers were exfoliated from bulk crystals and directly transferred, isolated, and aligned onto polyethylene terephthalate (PET) through micromechanical exfoliation as described in the Supporting Information (SI). Benefiting from the strong interaction between 1H-$MoTe_2$ and the PET substrate, the uniaxial strain applied to the PET surface is coherently transferred to 1H-$MoTe_2$ during the mechanical loading process (Figure 1b and Figure S1), up to the maximum applied strain. The zigzag edge formation energy (∼0.569 eV/Å) for 2H-$MoTe_2$ is lower than that of armchair edges (∼0.645 eV/Å).[44] Consequently, the 1H-$MoTe_2$ monolayers preferentially presents their edges along zigzag directions (Figure S3). Taking advantage of this phenomenon, the mechanical loading direction is finely controlled by identifying the clean zigzag edges, ensuring that the uniaxial strain is applied strictly along either the armchair or the zigzag direction to study the directional dependence.

Complementary metrology and spectroscopy measurements were used to isolate monolayer 1H-$MoTe_2$ crystals to study.

https://doi.org/10.1021/acs.nanolett.3c03706
Nano Lett. 2023, 23, 11763−11770

Raman spectra of mono-/bi-/tri-/quad-layer and bulk 2H-$MoTe_2$ crystals adhered to the PET surface (Figure 2a) were characterized and distinguished. PET itself does not have any Raman-active modes between 100 and 400 cm^{-1} where characteristic peaks of 1H-$MoTe_2$ are located. The Raman spectra of monolayer 1H-$MoTe_2$ was compared on PET and SiO_2/Si substrates. No significant differences in Raman peak positions and the full width at half-maximum (fwhm) for the monolayer 1H-$MoTe_2$ on both substrates were observed, indicating that PET is an appropriate substrate for studying the phonon behavior of 1H-$MoTe_2$ through Raman spectroscopy (Figure S2).

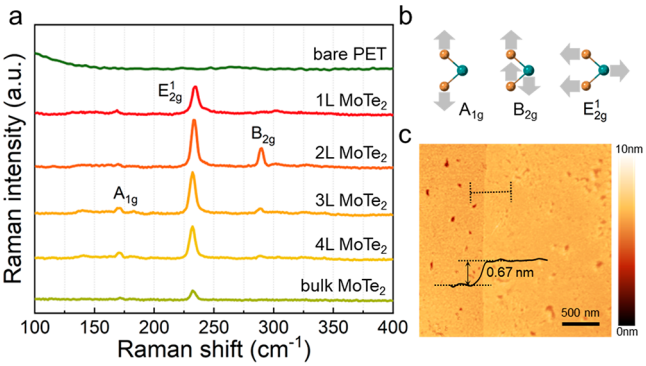

Figure 2. Identification of the monolayer 1H-$MoTe_2$. (a) Raman spectra of 1H/2H-$MoTe_2$ with different numbers of layers. The A_{1g} peak near 170 cm^{-1} and the E^1_{2g} peak near 231 cm^{-1} are characteristic peaks of the 1H phase. The B_{2g} vibration peak near 289 cm^{-1} is absent for bulk and monolayer $MoTe_2$ but activated in few-layer crystals due to the breaking of translational symmetry. (b) Schematic of the out-of-plane A_{1g} and B_{2g} vibrational modes and in-plane E^1_{2g} mode. Gray arrows indicate the vibration directions of atoms. (c) AFM image for monolayer 1H-$MoTe_2$ on PET and the height profile corresponding to the dotted line section, exhibiting an average step height of 0.67 ± 0.10 nm.

Three Raman-active peaks are present for 1H/2H-$MoTe_2$,[45] corresponding to two out-of-plane vibrational modes and one in-plane vibrational mode (Figure 2b). The out-of-plane A_{1g} mode entails the mutual vibration of two Te atoms in the basal plane. The out-of-plane B_{2g} mode involves the vibrational interaction between Te and Mo atoms within the same layer, exhibiting a 180° phase difference from the adjacent layers. As for the in-plane E^1_{2g} vibrational mode, the Mo and Te atoms oscillate opposite to one another within the same layer.[46] With an increasing number of layers in a crystal, the Raman intensities for E^1_{2g} peaks first increase for up to ∼3 layers and then decrease for thicker crystals. This trend in $MoTe_2$ has been interpreted to be due to the combination of optical field enhancements by the substrate, optical interference, and varying force constants between inner and outer layers.[47] Similar phenomena have also been observed for other TMDCs including MoS_2[48] and WTe_2.[49] The B_{2g} peak near 289 cm^{-1} is absent in monolayer and bulk 1H/2H-$MoTe_2$ but activated in few-layer crystals due to breaking of the translational symmetry.[45,50] Monolayer crystals that exhibit Raman signatures with the absence of the B_{2g} peak while demonstrating a strong E^1_{2g} peak were additionally verified for their single-layer thinness via atomic force microscopy (AFM). The measured step height from the PET substrate to the monolayer 1H-$MoTe_2$ surface is ∼0.67 ± 0.10 nm, consistent with the reported interlayer separation range (0.6–0.65 nm).[7]

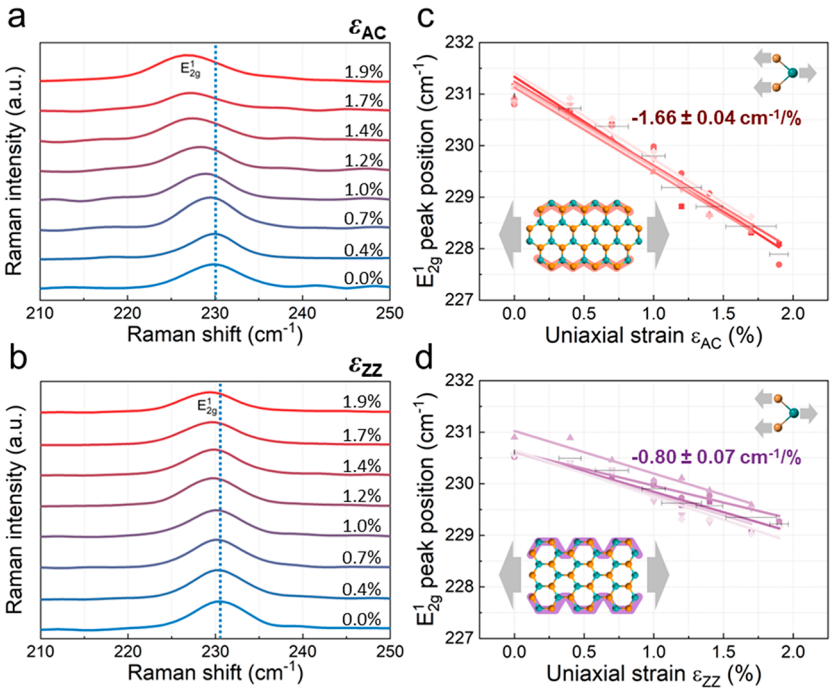

Figure 3. Evolution in the Raman spectra of monolayer 1H-$MoTe_2$ under applied uniaxial tensile strain along the (a, c) armchair direction and (b, d) zigzag direction. The initial E^1_{2g} peak position with no applied strain is marked with a blue vertical dashed line. The E^1_{2g} peak position consistently red-shifts with increasing tensile strain along both the (c) armchair direction and (d) zigzag direction across all samples, exhibiting average shifts of −1.66 ± 0.04 and −0.80 ± 0.07 cm^{-1}/%, respectively. Insets illustrate the E^1_{2g} vibrational mode of monolayer 1H-$MoTe_2$ and applied strain directions with respect to the crystal lattices.

https://doi.org/10.1021/acs.nanolett.3c03706
Nano Lett. 2023, 23, 11763−11770

The PET substrate is subjected to bending via a custom apparatus (Figure S1), yielding purely uniaxial tensile strain applied to the surface 1H-$MoTe_2$ monolayers. This uniaxial tensile strain applied to the surface 1H-$MoTe_2$ monolayers is estimated by the maximum tensile strain on the surface of the PET substrate, following the relation[51] $\varepsilon = \kappa \cdot t/2$, where t is the thickness of the PET substrate (~0.79 mm) and κ is the curvature of the localized region where the monolayer 1H-$MoTe_2$ is attached. The applied tensile strain was also confirmed from top-view optical images via edge detection by tracking the lateral deformation of 1H-$MoTe_2$ monolayers (Table. S1).[52] The applied strain quantified by either of the two measurements are nearly identical with a maximum deviation of <0.2% strain (as described in the SI).

In situ micro-Raman spectroscopy was used to monitor the phonon response of monolayer 1H-$MoTe_2$ to varying uniaxial strains along distinct crystallographic directions. With no strain applied, a prominent Raman peak for the E^1_{2g} mode at ~231 cm^{-1} is observed (Figure 3a). Under progressively increasing uniaxial strains up to 1.9% along the armchair direction, the E^1_{2g} peak monotonically red-shifts with a rate of −1.66 ± 0.04 cm^{-1}/% (Figure 3c). The lower Raman frequency concomitant with larger applied uniaxial strain is attributed to lattice expansion and decay into lower energy phonons.[53] At even higher applied strains, fracture occurs in some of the 1H-$MoTe_2$ monolayers, leading to the strain release reflected by an abrupt blue shift of the E^1_{2g} peak (Figure S4). When subjected to tensile strain along the zigzag direction, the E^1_{2g} peak exhibits a comparatively more gradual red shift with a rate of −0.80 ± 0.07 cm^{-1}/% (Figure 3b,d). The strain-coupled phonon evolution in 1H-$MoTe_2$ along the zigzag direction is weaker compared to the armchair direction, which is consistent with the directionally anisotropic phase energy landscape of $MoTe_2$ under uniaxial strain.[31] Apart from $MoTe_2$, other 2D Mo- and W-dichalcogenides such as MoS_2, $MoSe_2$, WS_2, WSe_2, and WTe_2 have all been computationally predicted to exhibit a similar directionally resolved strain-coupled phonon response.[54,55] Experimentally, strain-induced phonon softening has been reported for all these 2D transition-metal sulfides and selenides,[56−59] while direction dependence has only been reported for MoS_2 thus far.[60] The protocol established for strain modulation developed in this work, including control over the layer number and lattice orientation, serves as a benchmark for future investigations of the phonon properties of other TMDCs and the ever-growing repertoire of 2D materials more generally.

Due to the empirical nature of the micromechanical exfoliation and transfer process of $MoTe_2$ crystals, some flakes may yield residual strain distributions which makes their initial E^1_{2g} peak position deviate from 231 cm^{-1}. Therefore, only "strain-free" samples with an initial E^1_{2g} peak position close to 231 cm^{-1} were selected and subjected to strain engineering and characterization. The average initial E^1_{2g} peak position for all of the measured samples is 230.82 ± 0.13 cm^{-1}. A tight agreement in the rate of red-shift can be seen among different monolayer samples screened (Figure 3c,d), despite small deviations in the initial E^1_{2g} peak position.

To further quantify the strain-coupling with the phonon vibrational modes, the fwhm of the evolving E^1_{2g} mode (Figure 4c,d) was extracted from the Raman spectra under various uniaxial tensile strains along both armchair and zigzag directions (Figure 4a,b). Only a tiny amount of broadening was observed during the strain loading process with the fwhm

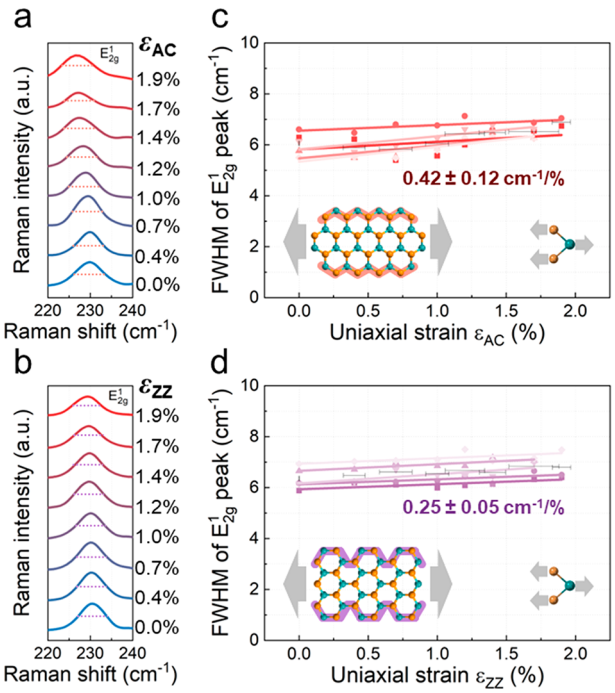

Figure 4. Full width at half-maximum (fwhm) of the E^1_{2g} Raman peak for monolayer 1H-$MoTe_2$ under applied uniaxial tensile strains along the (a) armchair direction and (b) zigzag direction. The fwhm of the E^1_{2g} Raman peak remains relatively unchanged for increasing tensile strains both along the (c) armchair direction and (d) zigzag direction, exhibiting average increases of 0.42 ± 0.12 and 0.25 ± 0.05 cm^{-1}/%, respectively. Insets illustrate the E^1_{2g} vibrational mode of monolayer 1H-$MoTe_2$ and applied strain directions with respect to the crystal lattices.

broadening at a rate of 0.42 ± 0.12 cm^{-1}/% for the armchair direction and 0.25 ± 0.05 cm^{-1}/% for the zigzag direction. The normalized maximum broadening in the fwhm is 11% for the armchair direction and 7% for the zigzag direction. This small amount of broadening is unlikely to be due to the emergence of new Raman modes as a result of phase transitions (such as in the 1T′ phase). A possible reason could be modifications in the dielectric environment, potentially impacting phenomena such as interfacial band bending.[61] This very small broadening of the fwhm further substantiates that no phase transition occurred in monolayer 1H-$MoTe_2$ under uniaxial tensile strain up to 1.9%, along neither the armchair direction nor the zigzag direction.

The Grüneisen parameter (γ) is a key parameter that quantifies the coupling strength between the applied strain (lattice distortion) and the resultant shift in the phonon frequency. By extracting the strain-dependent Raman spectra, the directionally resolved Grüneisen parameters can be experimentally determined for monolayer 1H-$MoTe_2$. Through uniaxial strain, the Grüneisen parameters are calculated as[62]

$$\gamma_{E_{2g}} = -\frac{\Delta\omega^{+}_{E_{2g}} + \Delta\omega^{-}_{E_{2g}}}{2\omega^{0}_{E_{2g}}(1-\nu)\varepsilon}$$

where $\omega^0_{E_{2g}}$ is the intrinsic E^1_{2g} peak position at zero strain, $\triangle\omega^{\pm}_{E_{2g}}$ is the shift of the E^1_{2g} phonon due to ε the uniaxial strain in the crystal (± indicates the shift direction relative to zero strain), and ν is the in-plane Poisson ratio of 1H-$MoTe_2$

https://doi.org/10.1021/acs.nanolett.3c03706
Nano Lett. 2023, 23, 11763−11770

(previously estimated to be ~0.25 for both armchair and zigzag directions[63,64]). When uniaxial tensile strain is applied to an ideal freestanding 1H-$MoTe_2$ (along the longitudinal direction), the intrinsic Poisson effect causes the material to contract in the lateral "perpendicular" direction. However, the strong adhesion between monolayer 1H-$MoTe_2$ and the PET substrates[65] over the entire range of applied strains in this study (up to ~1.9%) ensures coherent deformation and strain transfer between the PET substrate surface and the 1H-$MoTe_2$ monolayers. The Poisson effect from the PET (Poisson ratio of ~0.34) is inherited by 1H-$MoTe_2$ and is considered here for the Grüneisen parameter estimation. Given that no observable peak splitting was observed for any of the monolayer 1H-$MoTe_2$ under various strains (as evidenced by the consistent fwhm of the E^1_{2g} peaks), the as-measured E^1_{2g} phonon shift is considered to originate from a single vibrational mode (E^1_{2g}). Therefore, in the absence of any peak split, the $\Delta\omega^+_{E_{2g}} + \Delta\omega^-_{E_{2g}}$ term can be simplified to $2\Delta\omega_{E_{2g}}$, and the equation can be rewritten as[66]

$$\gamma_{E_{2g}} = -\frac{\Delta\omega_{E_{2g}}}{\omega^0_{E_{2g}}(1-\nu)\varepsilon}$$

Based on the empirically measured results, the E^1_{2g} mode Grüneisen parameters for monolayer 1H-$MoTe_2$ are estimated to be $\gamma_{E_{2g}(AC)} = 1.09 \pm 0.03$ along the armchair direction and $\gamma_{E_{2g}(ZZ)} = 0.52 \pm 0.04$ along the zigzag direction. The positive γ values with increasing in-plane tensile uniaxial strain indicate a decrease in frequencies (phonon softening),[67] which is consistent with the fact that the E^1_{2g} vibration belongs to in-plane acoustic modes. To the best of our knowledge, this is the first empirically derived estimation of the directionally dependent Grüneisen parameters in monolayer 1H-$MoTe_2$, and these values fall within the range of computationally derived results (0.52−0.99) reported thus far (Table S3).[36,64,68] Moreover, according to the Slack model, the lattice thermal conductivity is inversely related to the Grüneisen parameter. Given these empirically derived anisotropic Grüneisen parameters, an inference can be drawn that 1H-$MoTe_2$ exhibits anisotropic and higher basal-plane thermal conductivity in the zigzag direction compared to the armchair direction. This inference of the anisotropic in-plane thermal conductivity is consistent with previous DFT calculations.[64] It is worth noting that first-principles studies have suggested that anisotropy in the basal plane thermal conductivity exists in $1T'/T_d$-$MoTe_2$ but not in 2H-$MoTe_2$ due to crystal symmetry.[68,69] However, the lateral symmetry of 1H/2H-$MoTe_2$ is broken upon application of uniaxial strains, leading to a disparity in the frequency of dominant heat-carrying phonons along different lateral directions. Therefore, these results are not in conflict with each other.

As previously mentioned, the discrepancies in the strain-coupled phonon evolution of $MoTe_2$ between computational and empirical studies thus far are mainly due to the mismatch in their applied strain conditions and crystal configurations (Figure 5). Before this present work, all the reported experimental results (whether uniaxially or biaxially applied strain) have neglected crystal orientation, and none of these studies were based on monolayer 1H-$MoTe_2$ (they were all 2−100 layers). As a result, there exist large inconsistencies between the empirically measured versus computationally derived strain-coupled E^1_{2g} phononic properties. To the best of our knowledge, this work is the first to empirically quantify the E^1_{2g} phonon evolution of monolayer 1H-$MoTe_2$ under uniaxial tensile strain along both armchair and zigzag directions.

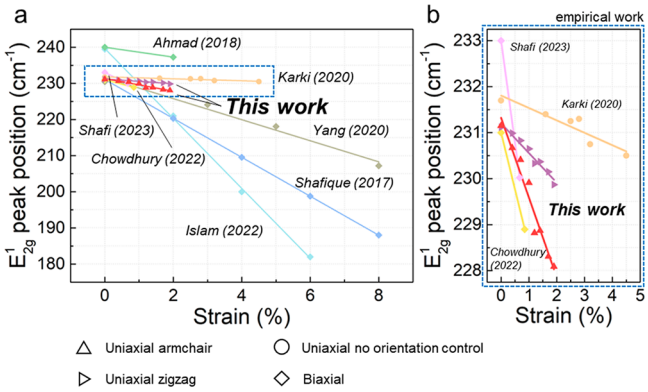

Figure 5. Summary of strain−phonon coupling of the E^1_{2g} phonon mode in 2H-$MoTe_2$ reported in the literature. This present study is the first to empirically quantify the E^1_{2g} phonon evolution of monolayer 1H-$MoTe_2$ (red and purple plots in (a) and (b)). This is also the first study to delineate between uniaxially applied tensile strain along the armchair and the zigzag directions to reveal 1H-$MoTe_2$'s directionally dependent phononic properties.[8,18,27−31,33−36,70]

In summary, the directionally dependent strain−phonon coupling of monolayer 1H-$MoTe_2$ under uniaxial tensile strain is quantified for the first time. The characteristic phonon modes were measured with respect to uniaxial strain via in situ micro-Raman spectroscopy, with the E^1_{2g} peak monotonically red-shifting at rates of -1.66 ± 0.04 and -0.80 ± 0.07 cm^{-1}/% along the armchair and the zigzag directions, respectively. Moreover, the calculated Grüneisen parameters of $\gamma_{E_{2g}(AC)} = 1.09 \pm 0.03$ along the armchair direction and $\gamma_{E_{2g}(ZZ)} = 0.52 \pm 0.04$ along the zigzag direction provide an empirical benchmark for future strain engineering efforts of $MoTe_2$ and other 2D transition-metal tellurides. This work provides the first rigorous characterization of the anisotropic strain-induced phonon response in monolayer 1H-$MoTe_2$, and it finally clarifies the disparities between previously reported experimental observations and computational results.

■ ASSOCIATED CONTENT

Supporting Information

Details on sample preparation, metrology and spectroscopy, data analysis, are provided in the Supporting Information document. The Supporting Information is available free of charge at https://pubs.acs.org/doi/10.1021/acs.nanolett.3c03706.

(PDF)

■ AUTHOR INFORMATION

Corresponding Author

Michael Cai Wang − *Department of Mechanical Engineering, Department of Medical Engineering, and Department of Chemical, Biological, and Materials Engineering, University of South Florida, Tampa, Florida 33620, United States;* orcid.org/0000-0003-3300-852X; Email: mcwang@usf.edu

https://doi.org/10.1021/acs.nanolett.3c03706
Nano Lett. 2023, 23, 11763−11770

Authors

Zhewen Yin − *Department of Mechanical Engineering, University of South Florida, Tampa, Florida 33620, United States;* orcid.org/0000-0002-6855-6799

Wyatt Panaccione − *Department of Mechanical Engineering, University of South Florida, Tampa, Florida 33620, United States;* Present Address: Department of Mechanical and Aerospace Engineering, The Ohio State University, Columbus, Ohio, 43210, United States

Anjun Hu − *Department of Medical Engineering, University of South Florida, Tampa, Florida 33620, United States*

Ossie R. T. Douglas − *Department of Mechanical Engineering, University of South Florida, Tampa, Florida 33620, United States*

Md Rubayat-E Tanjil − *Department of Mechanical Engineering, University of South Florida, Tampa, Florida 33620, United States*

Yunjo Jeong − *Department of Mechanical Engineering, University of South Florida, Tampa, Florida 33620, United States;* Present Address: Functional Composite Materials Research Center, Korea Institute of Science and Technology, Jeonbuk, 55324, South Korea.

Huijuan Zhao − *Department of Mechanical Engineering, Clemson University, Clemson, South Carolina 29634-0921, United States;* orcid.org/0000-0002-9714-4515

Complete contact information is available at: https://pubs.acs.org/10.1021/acs.nanolett.3c03706

Author Contributions

Z.Y., H.Z., and M.C.W. designed the research, Z.Y., W.P., A.H., M.R.T., and O.R.T.D. performed research, Z.Y., H.Z., and M.C.W. analyzed data, and Z.Y., W.P., A.H., O.R.T.D., M.R.T., Y.J., H.Z., and M.C.W. wrote the manuscript.

Notes

The authors declare no competing financial interest.

■ ACKNOWLEDGMENTS

Experiments were performed at the University of South Florida Nanotechnology Research and Education Center (NREC) with assistance from Robert Tufts, Richard Everly, Yusuf Emirov, and Jay Bieber. We acknowledge support from the ORAU Ralph E. Powe Junior Faculty Enhancement Award. This material is based upon work supported in part by the National Science Foundation under grant no. CMMI-1944638 (CMMI Advanced Manufacturing). Acknowledgment is made to the Donors of the American Chemical Society Petroleum Research Fund for partial support of this research (PRF# 62293-DNI5). H.Z. acknowledges support from the Department of Energy (DOE) under Award Number DE-FE0031765. O.R.T.D. acknowledges support from the NASA Space Technology Graduate Research Opportunity (80NSSC22K1216), University of South Florida Florida-Georgia Louis Stokes Alliance for Minority Participation (FGLSAMP) (HRD-1906518), Alfred P. Sloan Minority Graduate Scholarship Program, and the National GEM Consortium Fellowship.

■ REFERENCES

(1) Biswas, S.; Champagne, A.; Haber, J. B.; Pokawanvit, S.; Wong, J.; Akbari, H.; Krylyuk, S.; Watanabe, K.; Taniguchi, T.; Davydov, A. V.; Al Balushi, Z. Y.; Qiu, D. Y.; da Jornada, F. H.; Neaton, J. B.; Atwater, H. A. Rydberg Excitons and Trions in Monolayer $MoTe_2$. *ACS Nano* **2023**, *17* (8), 7685−7694.

(2) Wang, W.; Kim, S.; Liu, M.; Cevallos, F. A.; Cava, R. J.; Ong, N. P. Evidence for an Edge Supercurrent in the Weyl Superconductor $MoTe_2$. *Science* **2020**, *368* (6490), 534−537.

(3) Jindal, A.; Saha, A.; Li, Z.; Taniguchi, T.; Watanabe, K.; Hone, J. C.; Birol, T.; Fernandes, R. M.; Dean, C. R.; Pasupathy, A. N.; Rhodes, D. A. Coupled Ferroelectricity and Superconductivity in Bilayer Td-$MoTe_2$. *Nature* **2023**, *613* (7942), 48−52.

(4) Anderson, E.; Fan, F.-R.; Cai, J.; Holtzmann, W.; Taniguchi, T.; Watanabe, K.; Xiao, D.; Yao, W.; Xu, X. Programming Correlated Magnetic States with Gate-Controlled Moiré Geometry. *Science* **2023**, *381*, No. eadg4268.

(5) Cai, J.; Anderson, E.; Wang, C.; Zhang, X.; Liu, X.; Holtzmann, W.; Zhang, Y.; Fan, F.; Taniguchi, T.; Watanabe, K.; Ran, Y.; Cao, T.; Fu, L.; Xiao, D.; Yao, W.; Xu, X. Signatures of Fractional Quantum Anomalous Hall States in Twisted $MoTe_2$. *Nature* **2023**, *622*, 63−68.

(6) Keum, D. H.; Cho, S.; Kim, J. H.; Choe, D. H.; Sung, H. J.; Kan, M.; Kang, H.; Hwang, J. Y.; Kim, S. W.; Yang, H.; Chang, K. J.; Lee, Y. H. Bandgap Opening in Few-Layered Monoclinic $MoTe_2$. *Nat. Phys.* **2015**, *11* (6), 482−486.

(7) Ruppert, C.; Aslan, O. B.; Heinz, T. F. Optical Properties and Band Gap of Single- and Few-Layer $MoTe_2$ Crystals. *Nano Lett.* **2014**, *14* (11), 6231−6236.

(8) Huang, H. H.; Fan, X.; Singh, D. J.; Chen, H.; Jiang, Q.; Zheng, W. T. Controlling Phase Transition for Single-Layer MTe_2(M = Mo and W): Modulation of the Potential Barrier under Strain. *Phys. Chem. Chem. Phys.* **2016**, *18* (5), 4086−4094.

(9) Saito, R.; Tatsumi, Y.; Huang, S.; Ling, X.; Dresselhaus, M. S. Raman Spectroscopy of Transition Metal Dichalcogenides. *J. Phys.: Condens. Matter* **2016**, *28* (35), No. 353002.

(10) Park, J.; Kim, Y.; Jhon, Y. I.; Jhon, Y. M. Temperature Dependent Raman Spectroscopic Study of Mono-, Bi-, and Tri-Layer Molybdenum Ditelluride. *Appl. Phys. Lett.* **2015**, *107* (15), 16.

(11) Cheon, Y.; Lim, S. Y.; Kim, K.; Cheong, H. Structural Phase Transition and Interlayer Coupling in Few-Layer 1T′ and Td $MoTe_2$. *ACS Nano* **2021**, *15* (2), 2962−2970.

(12) Yang, D.; Hu, X.; Zhuang, M.; Ding, Y.; Zhou, S.; Li, A.; Yu, Y.; Li, H.; Luo, Z.; Gan, L.; Zhai, T.; et al. Inversion Symmetry Broken 2D 3R-$MoTe_2$. *Adv. Funct Mater.* **2018**, *28* (26), No. 1800785.

(13) Ma, T.; Chen, H.; Yananose, K.; Zhou, X.; Wang, L.; Li, R.; Zhu, Z.; Wu, Z.; Xu, Q.-H.; Yu, J.; Qiu, C. W.; Stroppa, A.; Loh, K. P. Growth of Bilayer $MoTe_2$ Single Crystals with Strong Non-Linear Hall Effect. *Nat. Commun.* **2022**, *13* (1), 5465.

(14) Rhodes, D. A.; Jindal, A.; Yuan, N. F. Q.; Jung, Y.; Antony, A.; Wang, H.; Kim, B.; Chiu, Y. C.; Taniguchi, T.; Watanabe, K.; Barmak, K.; Balicas, L.; Dean, C. R.; Qian, X.; Fu, L.; Pasupathy, A. N.; Hone, J. Enhanced Superconductivity in Monolayer Td-$MoTe_2$. *Nano Lett.* **2021**, *21* (6), 2505−2511.

(15) Szary, M. J.; Florjan, D. M.; Bąbelek, J. A. Selective Detection of Carbon Monoxide on P-Block Doped Monolayers of $MoTe_2$. *ACS Sens* **2022**, *7* (1), 272−285.

(16) Park, S.; Jeong, Y.; Jin, H.-J.; Park, J.; Jang, H.; Lee, S.; Huh, W.; Cho, H.; Shin, H. G.; Kim, K.; Lee, C.-H.; Choi, S.; Im, S. Nonvolatile and Neuromorphic Memory Devices Using Interfacial Traps in Two-Dimensional WSe_2 /$MoTe_2$ Stack Channel. *ACS Nano* **2020**, *14* (9), 12064−12071.

(17) Wang, Y.; Zhang, M.; Xue, Z.; Chen, X.; Mei, Y.; Chu, P. K.; Tian, Z.; Wu, X.; Di, Z. Atomistic Observation of the Local Phase Transition in $MoTe_2$ for Application in Homojunction Photodetectors. *Small* **2022**, *18* (19), No. 2200913.

(18) Song, S.; Keum, D. H.; Cho, S.; Perello, D.; Kim, Y.; Lee, Y. H. Room Temperature Semiconductor−Metal Transition of $MoTe_2$ Thin Films Engineered by Strain. *Nano Lett.* **2016**, *16* (1), 188−193.

(19) Empante, T. A.; Zhou, Y.; Klee, V.; Nguyen, A. E.; Lu, I.-H.; Valentin, M. D.; Naghibi Alvillar, S. A.; Preciado, E.; Berges, A. J.; Merida, C. S.; Gomez, M.; Bobek, S.; Isarraraz, M.; Reed, E. J.; Bartels, L. Chemical Vapor Deposition Growth of Few-Layer $MoTe_2$ in the 2H, 1T′, and 1T Phases: Tunable Properties of $MoTe_2$ Films. *ACS Nano* **2017**, *11* (1), 900−905.

(20) Aslan, O. B.; Datye, I. M.; Mleczko, M. J.; Sze Cheung, K.; Krylyuk, S.; Bruma, A.; Kalish, I.; Davydov, A. V.; Pop, E.; Heinz, T. F. Probing the Optical Properties and Strain-Tuning of Ultrathin $Mo_{1-x}W_xTe_2$. *Nano Lett.* **2018**, *18* (4), 2485−2491.
(21) Cho, S.; Kim, S.; Kim, J. H.; Zhao, J.; Seok, J.; Keum, D. H.; Baik, J.; Choe, D. H.; Chang, K. J.; Suenaga, K.; Kim, S. W.; Lee, Y. H.; Yang, H. Phase Patterning for Ohmic Homojunction Contact in $MoTe_2$. *Science* **2015**, *349* (6248), 625−628.
(22) Tan, Y.; Luo, F.; Zhu, M.; Xu, X.; Ye, Y.; Li, B.; Wang, G.; Luo, W.; Zheng, X.; Wu, N.; Yu, Y.; Qin, S.; Zhang, X. A. Controllable 2H-to-1T′ Phase Transition in Few-Layer $MoTe_2$. *Nanoscale* **2018**, *10* (42), 19964−19971.
(23) Li, Y.; Duerloo, K.-A. A. N.; Wauson, K.; Reed, E. J. Structural Semiconductor-to-Semimetal Phase Transition in Two-Dimensional Materials Induced by Electrostatic Gating. *Nat. Commun.* **2016**, *7* (1), No. 10671.
(24) Wang, Y. Y.; Xiao, J.; Zhu, H.; Li, Y.; Alsaid, Y.; Fong, K. Y.; Zhou, Y.; Wang, S.; Shi, W.; Wang, Y. Y.; Zettl, A.; Reed, E. J.; Zhang, X. Structural Phase Transition in Monolayer $MoTe_2$ Driven by Electrostatic Doping. *Nature* **2017**, *550* (7677), 487−491.
(25) Nan, H.; Jiang, J.; Xiao, S.; Chen, Z.; Luo, Z.; Zhang, L.; Zhang, X.; Qi, H.; Gu, X.; Wang, X.; Ni, Z. Soft Hydrogen Plasma Induced Phase Transition in Monolayer and Few-Layer $MoTe_2$. *Nanotechnology* **2019**, *30* (3), No. 034004.
(26) Zhang, K.; Bao, C.; Gu, Q.; Ren, X.; Zhang, H.; Deng, K.; Wu, Y.; Li, Y.; Feng, J.; Zhou, S. Raman Signatures of Inversion Symmetry Breaking and Structural Phase Transition in Type-II Weyl Semimetal $MoTe_2$. *Nat. Commun.* **2016**, *7* (1), No. 13552.
(27) Shafi, A. M.; Uddin, G.; Cui, X.; Ali, F.; Ahmed, F.; et al. Strain Engineering for Enhancing Carrier Mobility in $MoTe_2$ Field-Effect Transistors. *Adv. Sci.* **2023**, *10*, No. 2303437.
(28) Chowdhury, S. A.; Inzani, K.; Penã, T.; Dey, A.; Wu, S. M.; Griffin, S. M.; Askari, H. Mechanical Properties and Strain Transfer Behavior of Molybdenum Ditelluride ($MoTe_2$) Thin Films. *Journal of Engineering Materials and Technology* **2022**, *144* (1), No. 011006.
(29) Karki, B.; Freelon, B.; Rajapakse, M.; Musa, R.; Riyadh, S. M. S.; Morris, B.; Abu, U.; Yu, M.; Sumanasekera, G.; Jasinski, J. B. Strain-Induced Vibrational Properties of Few Layer Black Phosphorus and $MoTe_2$ via Raman Spectroscopy. *Nanotechnology* **2020**, *31* (42), No. 425707.
(30) Hou, W.; Azizimanesh, A.; Sewaket, A.; Peña, T.; Watson, C.; Liu, M.; Askari, H.; Wu, S. M. Strain-Based Room-Temperature Non-Volatile $MoTe_2$ Ferroelectric Phase Change Transistor. *Nat. Nanotechnol* **2019**, *14* (7), 668−673.
(31) Duerloo, K. A. N.; Li, Y.; Reed, E. J. Structural Phase Transitions in Two-Dimensional Mo-and W-Dichalcogenide Monolayers. *Nat. Commun.* **2014**, *5* (1), 4214.
(32) Ghasemi, A.; Gao, W. Atomistic Mechanism of Stress Modulated Phase Transition in Monolayer $MoTe_2$. *Extreme Mech Lett.* **2020**, *40*, No. 100946.
(33) Islam, M. R.; Mojumder, M. R. H.; Moghal, B. K.; Islam, A. S. M. J.; Miah, M. R.; Roy, S.; Kumar, A.; Shihavuddin, A. S. M.; Ashique, R. H. Impact of Strain on the Electronic, Phonon, and Optical Properties of Monolayer Transition Metal Dichalcogenides XTe_2 (X = Mo and W). *Phys. Scr.* **2022**, *97* (4), No. 045806.
(34) Yang, W.; Zhu, L. Y.; Zhou, T.; Yang, T. J.; Yan, Y. B.; Li, J. J.; Zheng, F. W.; Yang, Y.; Wang, X. H.; Xu, W. B.; Zhang, P. Vibration Response of Monolayer 1H-$MoTe_2$ to Equibiaxial Strain. *Phys. Rev. B* **2020**, *102* (19), No. 195431.
(35) Ahmad, I.; Khan, S. A.; Idrees, M.; Haneef, M.; Shahid, I.; Din, H. U.; Khan, S. A.; Amin, B. Influence of Strain on Specific Features of MoX_2 (X = S, Se, Te) Monolayers. *Physica B Condens Matter* **2018**, *545*, 113−118.
(36) Shafique, A.; Shin, Y. H. Strain Engineering of Phonon Thermal Transport Properties in Monolayer 2H-$MoTe_2$. *Phys. Chem. Chem. Phys.* **2017**, *19* (47), 32072−32078.
(37) Cui, X.; Yan, X.; Wang, B.; Cai, Y. Phononic Transport in 1T′-$MoTe_2$: Anisotropic Structure with an Isotropic Lattice Thermal Conductivity. *Appl. Surf. Sci.* **2023**, *608*, No. 155238.
(38) Wu, W.; Wang, L.; Li, Y.; Zhang, F.; Lin, L.; Niu, S.; Chenet, D.; Zhang, X.; Hao, Y.; Heinz, T. F.; Hone, J.; Wang, Z. L. Piezoelectricity of Single-Atomic-Layer MoS_2 for Energy Conversion and Piezotronics. *Nature* **2014**, *514* (7523), 470−474.
(39) Wu, W.; Wang, L.; Yu, R.; Liu, Y.; Wei, S. H.; Hone, J.; Wang, Z. L. Piezophototronic Effect in Single-Atomic-Layer MoS_2 for Strain-Gated Flexible Optoelectronics. *Adv. Mater.* **2016**, *28* (38), 8463−8468.
(40) Li, D.; Wei, C.; Song, J.; Huang, X.; Wang, F.; Liu, K.; Xiong, W.; Hong, X.; Cui, B.; Feng, A.; Jiang, L.; Lu, Y. Anisotropic Enhancement of Second-Harmonic Generation in Monolayer and Bilayer MoS_2 by Integrating with TiO_2 Nanowires. *Nano Lett.* **2019**, *19* (6), 4195−4204.
(41) Wilson, J. A.; Yoffe, A. D. The Transition Metal Dichalcogenides Discussion and Interpretation of the Observed Optical, Electrical and Structural Properties. *Adv. Phys.* **1969**, *18* (73), 193−335.
(42) Gong, L.; Kinloch, I. A.; Young, R. J.; Riaz, I.; Jalil, R.; Novoselov, K. S. Interfacial Stress Transfer in a Graphene Monolayer Nanocomposite. *Adv. Mater.* **2010**, *22* (24), 2694−2697.
(43) Frisenda, R.; Drüppel, M.; Schmidt, R.; Michaelis de Vasconcellos, S.; Perez de Lara, D.; Bratschitsch, R.; Rohlfing, M.; Castellanos-Gomez, A. Biaxial Strain Tuning of the Optical Properties of Single-Layer Transition Metal Dichalcogenides. *NPJ. 2D Mater. Appl.* **2017**, *1* (1), 10.
(44) Sun, Y.; Pan, J.; Zhang, Z.; Zhang, K.; Liang, J.; Wang, W.; Yuan, Z.; Hao, Y.; Wang, B.; Wang, J.; Wu, Y.; Zheng, J.; Jiao, L.; Zhou, S.; Liu, K.; Cheng, C.; Duan, W.; Xu, Y.; Yan, Q.; et al. Elastic Properties and Fracture Behaviors of Biaxially Deformed, Polymorphic $MoTe_2$. *Nano Lett.* **2019**, *19* (2), 761−769.
(45) Yamamoto, M.; Wang, S. T.; Ni, M.; Lin, Y.-F.; Li, S.-L.; Aikawa, S.; Jian, W.-B.; Ueno, K.; Wakabayashi, K.; Tsukagoshi, K. Strong Enhancement of Raman Scattering from a Bulk-Inactive Vibrational Mode in Few-Layer $MoTe_2$. *ACS Nano* **2014**, *8* (4), 3895−3903.
(46) Pan, Y.; Zahn, D. R. T. Raman Fingerprint of Interlayer Coupling in 2D TMDCs. *Nanomaterials* **2022**, *12* (22), 3949.
(47) Grzeszczyk, M.; Gołasa, K.; Zinkiewicz, M.; Nogajewski, K.; Molas, M. R.; Potemski, M.; Wysmołek, A.; Babiñski, A. Raman Scattering of Few-Layers $MoTe_2$. *2d Mater.* **2016**, *3* (2), No. 025010.
(48) Lee, C.; Yan, H.; Brus, L. E.; Heinz, T. F.; Hone, J.; Ryu, S. Anomalous Lattice Vibrations of Single- and Few-Layer MoS_2. *ACS Nano* **2010**, *4* (5), 2695−2700.
(49) Kim, Y.; Jhon, Y. I.; Park, J.; Kim, J. H.; Lee, S.; Jhon, Y. M. Anomalous Raman Scattering and Lattice Dynamics in Mono- and Few-Layer WTe_2. *Nanoscale* **2016**, *8* (4), 2309−2316.
(50) Huang, J. H.; Deng, K. Y.; Liu, P. S.; Wu, C. T.; Chou, C. T.; Chang, W. H.; Lee, Y. J.; Hou, T. H. Large-Area 2D Layered $MoTe_2$ by Physical Vapor Deposition and Solid-Phase Crystallization in a Tellurium-Free Atmosphere. *Adv. Mater. Interfaces* **2017**, *4* (17), No. 1700157.
(51) Conley, H. J.; Wang, B.; Ziegler, J. I.; Haglund, R. F.; Pantelides, S. T.; Bolotin, K. I. Bandgap Engineering of Strained Monolayer and Bilayer MoS_2. *Nano Lett.* **2013**, *13* (8), 3626−3630.
(52) Dadgar, A. M.; Scullion, D.; Kang, K.; Esposito, D.; Yang, E. H.; Herman, I. P.; Pimenta, M. A.; Santos, E. J. G.; Pasupathy, A. N. Strain Engineering and Raman Spectroscopy of Monolayer Transition Metal Dichalcogenides. *Chem. Mater.* **2018**, *30* (15), 5148−5155.
(53) Hart, T. R.; Aggarwal, R. L.; Lax, B. Temperature Dependence of Raman Scattering in Silicon. *Phys. Rev. B* **1970**, *1* (2), 638.
(54) Chang, C. H.; Fan, X.; Lin, S. H.; Kuo, J. L. Orbital Analysis of Electronic Structure and Phonon Dispersion in MoS_2, $MoSe_2$, WS_2, and WSe_2 Monolayers under Strain. *Phys. Rev. B* **2013**, *88* (19), No. 195420.
(55) Amin, B.; Kaloni, T. P.; Schwingenschlögl, U. Strain Engineering of WS_2, WSe_2, and WTe_2. *RSC Adv.* **2014**, *4* (65), 34561−34565.
(56) Rice, C.; Young, R. J.; Zan, R.; Bangert, U.; Wolverson, D.; Georgiou, T.; Jalil, R.; Novoselov, K. S. Raman-Scattering Measure-

ments and First-Principles Calculations of Strain-Induced Phonon Shifts in Monolayer MoS_2. *Phys. Rev. B* **2013**, *87* (8), No. 081307.
(57) Horzum, S.; Sahin, H.; Cahangirov, S.; Cudazzo, P.; Rubio, A.; Serin, T.; Peeters, F. M. Phonon Softening and Direct to Indirect Band Gap Crossover in Strained Single-Layer $MoSe_2$. *Phys. Rev. B* **2013**, *87* (12), No. 125415.
(58) Wang, Y.; Cong, C.; Yang, W.; Shang, J.; Peimyoo, N.; Chen, Y.; Kang, J.; Wang, J.; Huang, W.; Yu, T. Strain-Induced Direct−Indirect Bandgap Transition and Phonon Modulation in Monolayer WS_2. *Nano Res.* **2015**, *8* (8), 2562−2572.
(59) Tang, N.; Du, C.; Wang, Q.; Xu, H. Strain Engineering in Bilayer WSe_2 over a Large Strain Range. *Microelectron. Eng.* **2020**, *223*, No. 111202.
(60) Gan, Y.; Zhao, H. Chirality and Vacancy Effect on Phonon Dispersion of MoS_2 with Strain. *Phys. Lett. A* **2016**, *380* (5−6), 745−752.
(61) Peña, T.; Chowdhury, S. A.; Azizimanesh, A.; Sewaket, A.; Askari, H.; Wu, S. M. Strain Engineering 2D MoS_2 with Thin Film Stress Capping Layers. *2d Mater.* **2021**, *8* (4), No. 045001.
(62) Mohiuddin, T. M. G. G.; Lombardo, A.; Nair, R. R.; Bonetti, A.; Savini, G.; Jalil, R.; Bonini, N.; Basko, D. M.; Galiotis, C.; Marzari, N.; Novoselov, K. S.; Geim, A. K.; Ferrari, A. C. Uniaxial Strain in Graphene by Raman Spectroscopy: G Peak Splitting, Grüneisen Parameters, and Sample Orientation. *Phys. Rev. B* **2009**, *79* (20), No. 205433.
(63) Mortazavi, B.; Berdiyorov, G. R.; Makaremi, M.; Rabczuk, T. Mechanical Responses of Two-Dimensional $MoTe_2$; Pristine 2H, 1T and 1T′ and 1T′/2H Heterostructure. *Extreme Mech Lett.* **2018**, *20*, 65−72.
(64) Zhang, D.; Ren, W.; Wang, K.; Chen, S.; Zhang, L.; Ni, Y.; Zhang, G. A Thermal Conductivity Switch via the Reversible 2H-1T′ Phase Transition in Monolayer $MoTe_2$. *Chinese Physics B* **2023**, *32* (5), No. 050505.
(65) Li, J. M.; Liu, C.; Qiao, H. C.; Zhu, L. Y.; Chen, G.; Dai, X. D. Hot Embossing/Bonding of a Poly(Ethylene Terephthalate) (PET) Microfluidic Chip. *Journal of Micromechanics and Microengineering* **2008**, *18* (1), No. 015008.
(66) Cheng, Y. C.; Zhu, Z. Y.; Huang, G. S.; Schwingenschlögl, U. Grüneisen Parameter of the G Mode of Strained Monolayer Graphene. *Phys. Rev. B* **2011**, *83* (11), No. 115449.
(67) Hu, J.; Vanacore, G. M.; Cepellotti, A.; Marzari, N.; Zewail, A. H. Rippling Ultrafast Dynamics of Suspended 2D Monolayers, Graphene. *Proc. Natl. Acad. Sci.* **2016**, *113* (43), E6555−E6561.
(68) Shen, J.; Han, D.; Zhang, B.; Cao, R.; Liu, Y.; Zheng, S.; Li, H.; Jiang, Y.; Xue, Y.; Xue, M. First-Principles Study on Phonon Transport Properties of $MoTe_2$ and WTe_2 Monolayers in Different Phases. *Physica E* **2023**, *145*, 115509.
(69) Li, H.; Pandey, T.; Jiang, Y.; Gu, X.; Lindsay, L.; Kan Koh, Y. Origins of Heat Transport Anisotropy in $MoTe_2$ and Other Bulk van Der Waals Materials. *Materials Today Physics* **2023**, *37*, No. 101196.
(70) Zhao, Y.; Li, Y.; He, S.; Ma, F. Semiconductor-Semimetal Transition of $MoTe_2$ Monolayer Modulated by Charge-Injection and Strain Engineering. *Chem. Phys. Lett.* **2021**, *770*, No. 138473.

https://doi.org/10.1021/acs.nanolett.3c03706
Nano Lett. 2023, 23, 11763−11770